mTOR signaling in VIP neurons regulates circadian clock synchrony and olfaction

Dong Liu[a,1], Adam Stowie[b,1], Nuria de Zavalia[c,1], Tanya Leise[d], Salil Saurav Pathak[a], Lester R. Drewes[a], Alec J. Davidson[b], Shimon Amir[c,2], Nahum Sonenberg[e,f,g,2], and Ruifeng Cao[a,h,2]

[a]Department of Biomedical Sciences, University of Minnesota Medical School, Duluth, MN 55812; [b]Department of Neurobiology, Morehouse School of Medicine, Atlanta, GA 30310; [c]Center for Studies in Behavioral Neurobiology, Concordia University, Montreal, QC H4B 1R6, Canada; [d]Department of Mathematics and Statistics, Amherst College, Amherst, MA 01002; [e]Department of Biochemistry, McGill University, Montreal, QC H3A 1A3, Canada; [f]Goodman Cancer Research Center, McGill University, Montreal, QC H3A 1A3, Canada; [g]Howard Hughes Medical Institute, McGill University, Montreal, QC H3A 1A3, Canada; and [h]Department of Neuroscience, University of Minnesota Medical School, Minneapolis, MN 55455

Contributed by Nahum Sonenberg, February 12, 2018 (sent for review December 14, 2017; reviewed by Michael C. Antle and Illana Gozes)

Mammalian/mechanistic target of rapamycin (mTOR) signaling controls cell growth, proliferation, and metabolism in dividing cells. Less is known regarding its function in postmitotic neurons in the adult brain. Here we created a conditional *mTOR* knockout mouse model to address this question. Using the Cre-LoxP system, the *mTOR* gene was specifically knocked out in cells expressing *Vip* (vasoactive intestinal peptide), which represent a major population of interneurons widely distributed in the neocortex, suprachiasmatic nucleus (SCN), olfactory bulb (OB), and other brain regions. Using a combination of biochemical, behavioral, and imaging approaches, we found that mice lacking *mTOR* in VIP neurons displayed erratic circadian behavior and weakened synchronization among cells in the SCN, the master circadian pacemaker in mammals. Furthermore, we have discovered a critical role for mTOR signaling in mediating olfaction. Odor stimulated *mTOR* activation in the OB, anterior olfactory nucleus, as well as piriform cortex. Odor-evoked c-Fos responses along the olfactory pathway were abolished in mice lacking mTOR in VIP neurons, which is consistent with reduced olfactory sensitivity in these animals. Together, these results demonstrate that mTOR is a key regulator of SCN circadian clock synchrony and olfaction.

mTOR | VIP | SCN | circadian clock | olfaction

Almost all aspects of neuronal functions are regulated by external signals via intracellular signal transduction cascades. Mammalian/mechanistic target of rapamycin (mTOR) is an evolutionarily conserved serine/threonine protein kinase. Centered on mTOR, an intracellular signaling network controls cell growth, proliferation, and metabolism in dividing cells (1, 2). mTOR forms two multiprotein complexes, mTOR complex (mTORC) 1 and mTORC2. mTORC1 activates ribosomal protein S6 kinase (S6K) 1 and S6K2, which in turn phosphorylate the ribosomal protein S6 at Ser240/244 (3–5). mTOR signaling senses intracellular signals including nutrient availability, energy status, and stress, as well as responds to extracellular stimuli by hormones and growth factors. In the developing brain, mTOR signaling promotes neuronal progenitor proliferation, differentiation, and neural circuit formation (6). It is essential in early development, and homozygous *mTOR* knockout is embryonically lethal in mice (7, 8).

Due to a lack of genetic mouse models of the *mTOR* mutant, less is known regarding mTOR functions in postmitotic neurons in the adult brain. Studies of mTOR functions were performed using mutants of individual components within mTOR signaling or with pharmacological mTOR inhibitors. It is found that mTOR signaling controls synaptic plasticity, learning, and memory through its interaction with FKBP12 (FK506-binding protein), the mTORC1 downstream effector S6Ks, eukaryotic translation initiation factor 4E (eIF4E)-binding protein (4E-BP), and mTORC2 (9–12). mTOR signaling serves as a fuel sensor in the hypothalamus to regulate food intake (13). mTOR also modulates cortical plasticity during sleep and is involved in the effect of sleep deprivation on memory impairment (14, 15). Dysregulation of mTOR signaling pathways in the brain has frequently been identified in neurological and psychiatric disorders (6, 16).

Our previous study pointed to a role for mTOR in the hypothalamic suprachiasmatic nucleus (SCN), the master circadian pacemaker in mammals. The activities of mTORC1 in the SCN exhibit autonomous daily oscillations and are activated by light at night (17, 18). Inhibition of mTOR activity by the drug rapamycin modulates photic resetting of mouse circadian behavior (19). More recently, we have found that mTORC1 promotes mRNA translation of *Vip* (vasoactive intestinal peptide) via the translation repressor 4E-BP1 (20). VIP is a neuropeptide essential for coupling and synchronization of SCN neurons (21). To further study the functions of mTOR in the SCN as well as in other brain regions, we created a conditional *mTOR* knockout mouse using the Cre-LoxP system (22). $Mtor^{flx/flx}$ mice (20) were crossed to *Vip-Cre* mice (23) to specifically knock out *mTOR* in VIP cells. Using this model, we studied the functions of mTOR in the adult SCN and olfactory bulb (OB), two representative brain regions where VIP neurons are enriched. Using a combination of biochemical, behavioral, and imaging approaches, we demonstrate that mTOR signaling plays a critical role in regulating SCN cell synchrony and olfaction. These results reveal physiological functions of mTOR in the adult brain.

Significance

The mammalian/mechanistic target of rapamycin (mTOR) kinase resides at the crux of an intracellular signaling network that controls fundamental biological processes. Dysregulation of mTOR signaling is linked to neurological and psychiatric diseases. However, the physiological functions of mTOR signaling in the adult brain are not fully understood. In the current study, we discovered that mTOR in vasoactive intestinal peptide (VIP) neurons plays a key role in regulating neurophysiology in the brain circadian clock and the olfactory system. The conditional *mTOR* knockout mouse will be a useful model for future investigations of mTOR and/or VIP.

Author contributions: R.C. designed research; D.L., A.S., N.d.Z., S.S.P., and R.C. performed research; R.C. contributed new reagents/analytic tools; D.L., N.d.Z., T.L., and R.C. analyzed data; and A.S., T.L., L.R.D., A.J.D., S.A., N.S., and R.C. wrote the paper.

Reviewers: M.C.A., University of Calgary; and I.G., Tel Aviv University.

The authors declare no conflict of interest.

[1]D.L., A.S., and N.d.Z. contributed equally to this work.

[2]To whom correspondence may be addressed. Email: shimon.amir@concordia.ca, nahum.sonenberg@mcgill.ca, or rcao@umn.edu.

This article contains supporting information online at www.pnas.org/lookup/suppl/doi:10.1073/pnas.1721578115/-/DCSupplemental.

Results

***mTOR* Is Knocked Down in VIP Neurons.** To study the specific role of mTOR in VIP neurons, we crossed *Mtor*$^{flx/flx}$ mice to *Vip-Cre* mice to get *Mtor*$^{flx/flx}$*:Vip-Cre* mice. These animals developed normally, were fertile, and did not display gross abnormalities or reduced productivity. Nissl staining indicated that the histological morphology was normal, and the numbers of cells were not decreased in the examined brain regions including the SCN, OB, and piriform cortex in *Mtor*$^{flx/flx}$*:Vip-Cre* mice compared with *Mtor*$^{flx/flx}$ littermates (Fig. S1). As VIP neurons are enriched in the SCN (24), we first examined mTOR activities in this region by double immunolabeling of VIP and phosphorylated S6 (at Ser240/244; p-S6), a sensitive and specific marker of mTOR activities. We found that p-S6 was strongly expressed in the VIP-expressing cells as well as non-VIP cells in the SCN of *Mtor*$^{flx/flx}$ mice (Fig. 1*A*). In contrast, p-S6 expression was decreased in the ventral SCN of *Mtor*$^{flx/flx}$*:Vip-Cre* mice, where VIP neurons are located. As a result, the number of cells with colocalized expression of p-S6 and VIP was significantly decreased in the SCN of *Mtor*$^{flx/flx}$*:Vip-Cre* mice, indicating effective knockdown of mTOR activities in VIP neurons. The down-regulation of mTOR was specific, as the number of p-S6–positive non-VIP cells was not changed (Fig. 1 *A* and *B*). Next, by Western blotting, we found that mTOR and p-S6 levels were both decreased in the forebrain of *Mtor*$^{flx/flx}$*:Vip-Cre* mice. The level of prepro-VIP, the precursor protein of VIP, was also markedly reduced in the *Mtor*$^{flx/flx}$*:Vip-Cre* mice, whereas the level of the VIP receptor VPAC2 was not changed (Fig. 1 *C* and *D*). Together, these results demonstrate that mTOR was specifically knocked down in VIP neurons in the *Mtor*$^{flx/flx}$*:Vip-Cre* mice, and that as a result of mTOR knockdown the prepro-VIP level was also reduced, consistent with a role for mTOR in promoting mRNA translation of *Vip* (20).

***Mtor*$^{flx/flx}$*:Vip-Cre* Mice Exhibit Abnormal Circadian Behavior.** To investigate the functions of mTOR in VIP neurons in the SCN, we first characterized the behavioral phenotypes of the *Mtor*$^{flx/flx}$*:Vip-Cre* mice by recording their circadian wheel-running locomotor activities. Mice were entrained in a 12-h/12-h light/dark (LD) cycle for 7 d and released into constant darkness (DD) for 10 d (Fig. 2*A*). The *Mtor*$^{flx/flx}$*:Vip-Cre* mice were able to entrain to the 12-h/12-h LD cycle and exhibited typical free-running activity rhythms in DD. However, the circadian period in these rhythms was significantly shortened compared with *Mtor*$^{flx/flx}$ mice (*Mtor*$^{flx/flx}$*:Vip-Cre* vs. *Mtor*$^{flx/flx}$: 23.81 ± 0.03 h, $n = 20$ vs. 23.93 ± 0.02 h, $n = 20$, $t = 3.492$, $P = 0.0025$). After the animals were entrained in LD for 10 d, the LD cycle was abruptly advanced by 8 h. Both groups of mice were able to be reentrained to the shifted LD cycle, but the *Mtor*$^{flx/flx}$*:Vip-Cre* mice were reentrained more quickly than the *Mtor*$^{flx/flx}$ mice (*Mtor*$^{flx/flx}$*:Vip-Cre* vs. *Mtor*$^{flx/flx}$: 7.2 ± 0.35 d, $n = 20$ vs. 9.45 ± 0.49 d, $n = 20$, $t = 3.319$, $P = 0.0042$).

Next, the mice were released into constant light (LL) for 38 d. Prolonged exposure to LL lengthens the period of circadian behavior and induces arrhythmic behavior in some animals (25). We analyzed the behavioral rhythmicity of the mice using average Fourier periodograms. The average peak of the periodogram of the *Mtor*$^{flx/flx}$*:Vip-Cre* mice was lower than that of the *Mtor*$^{flx/flx}$ mice, indicating weakened rhythmicity in the *Mtor*$^{flx/flx}$*:Vip-Cre* mice

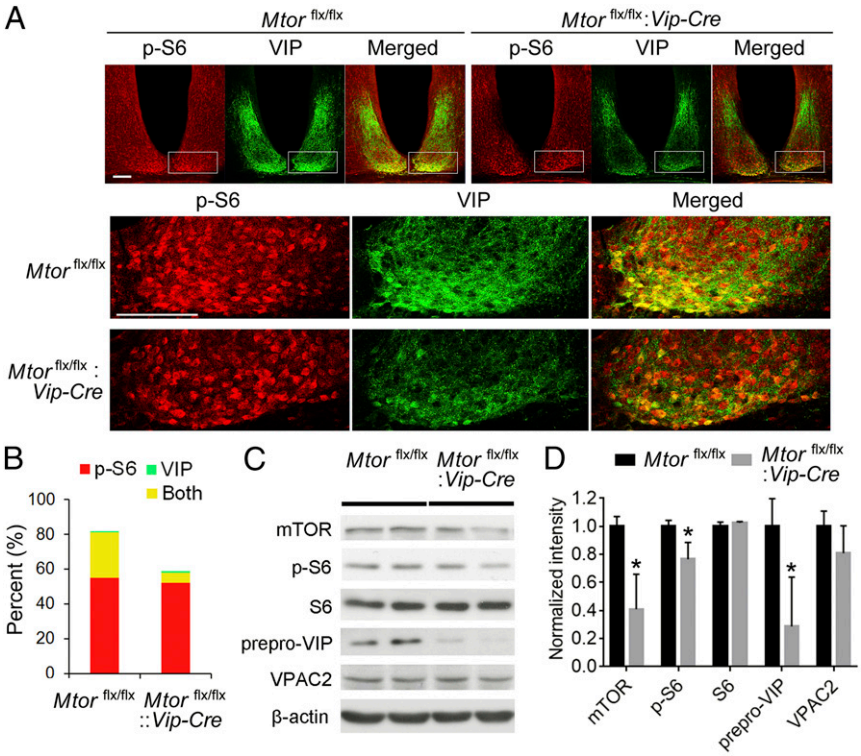

Fig. 1. *mTOR* is knocked down in VIP neurons in the SCN of *Mtor*$^{flx/flx}$*:Vip-Cre* mice. (*A*) Confocal microscopic images of immunofluorescent labeling for p-S6 (red) and VIP (green) in the suprachiasmatic nucleus. For these experiments, the mice were entrained to a 12-h/12-h light/dark cycle and killed at ZT6. p-S6 and VIP expression was colocalized in the ventral SCN in *Mtor*$^{flx/flx}$ mice. Note that the number of cells coexpressing p-S6 and VIP (yellow) was decreased in the SCN of the *Mtor*$^{flx/flx}$*:Vip-Cre* mice. Also note that intensities of p-S6 and VIP were both decreased in the ventral SCN. Framed regions are magnified and shown below. (Scale bars, 100 μm.) (*B*) Percentages of cells expressing p-S6, VIP, or both in the SCN. (*C*) Representative Western blots of forebrain lysates. (*D*) Quantitation of the blot intensities is shown. Values are presented as the mean ± SEM. Note that the level of prepro-VIP was markedly reduced in the *Mtor*$^{flx/flx}$*:Vip-Cre* brain but VPAC2 level was not changed. mTOR and p-S6 levels were also significantly reduced. Four *Mtor*$^{flx/flx}$ and four *Mtor*$^{flx/flx}$*:Vip-Cre* mice were used in the experiment. *$P < 0.05$ vs. *Mtor*$^{flx/flx}$.

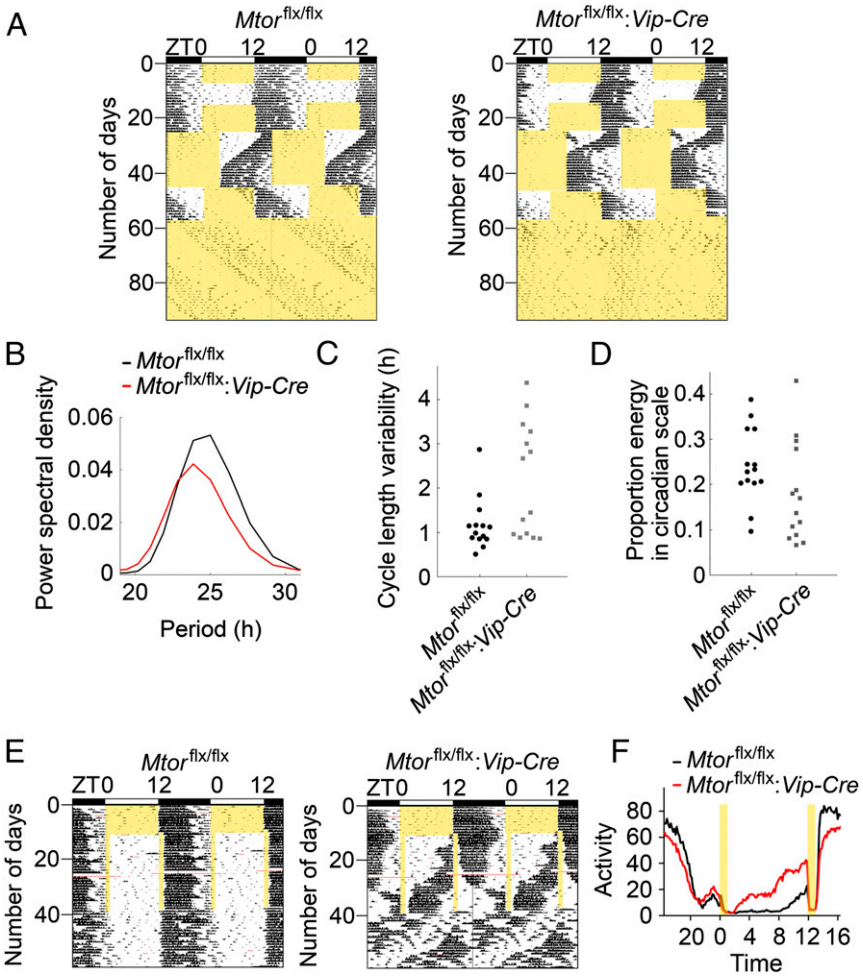

Fig. 2. Altered circadian behavior in *Mtor*$^{flx/flx}$*:Vip-Cre* mice. (*A*) Representative double-plotted actograms of mouse wheel-running activities from one *Mtor*$^{flx/flx}$ (*Left*) and one *Mtor*$^{flx/flx}$*:Vip-Cre* (*Right*) mouse. The *x* axis (*Top*) indicates the ZT of the day. The *y* axis (*Left*) indicates the number of days during the experiment. For these experiments, mice were first entrained to 12-h/12-h light/dark cycles for 7 d and then released into constant darkness for 10 d. Next, animals were reentrained to 12-h/12-h LD for 10 d, and then the LD cycle was abruptly advanced by 8 h. Twenty days later, the LD cycle was delayed by 8 h. After 11 d in the delayed LD cycle, the mice were released into constant light for 38 d. Yellow areas indicate light periods. (*B*) Averaged Fourier periodograms in LL from all mice. Fourteen *Mtor*$^{flx/flx}$ *and* 14 *Mtor*$^{flx/flx}$*:Vip-Cre* mice were used in the experiment. Note that the overall rhythmicity of the *Mtor*$^{flx/flx}$*:Vip-Cre* mice was weaker compared with the *Mtor*$^{flx/flx}$ mice, as indicated by a lower mean power spectral density (normalized to show proportion power at each frequency). (*C*) Cycle-to-cycle variability in period in LL is shown as individual values. (*D*) Proportion energy in circadian scale (indicating how well-consolidated activity is as a circadian rhythm) in LL is shown as individual values. (*E*) Representative double-plotted actograms of wheel-running activities from an *Mtor*$^{flx/flx}$ (*Left*) and *Mtor*$^{flx/flx}$*:Vip-Cre* (*Right*) mouse. For this experiment, the mice were entrained to a 12-h/12-h LD cycle for 10 d, exposed to a skeleton photoperiod (1-h/11-h/1-h/11-h LDLD) for 28 d, and then released into DD for 21 d. Five *Mtor*$^{flx/flx}$ and seven *Mtor*$^{flx/flx}$*:Vip-Cre* mice were used in the experiment. Yellow areas indicate light periods. (*F*) Average activities (rev per 10 min) during the skeleton photoperiod from all of the mice.

(Fig. 2*B*). We also analyzed the rhythmicity using a discrete wavelet transform, which decomposes the activities into circadian and ultradian components. We used the following two measures (26): (*i*) cycle-to-cycle variability in period (SD in time between peaks for the circadian component of activity), an indicator of rhythm stability; and (*ii*) proportion of variance in the activity time series accounted for by the circadian component, which indicates how well-consolidated activity is as a circadian rhythm. A permutation test showed that the cycle-to-cycle variability was significantly higher in the *Mtor*$^{flx/flx}$*:Vip-Cre* mice than the *Mtor*$^{flx/flx}$ mice ($P = 0.006$; Fig. 2*C*), indicating less stability of rhythmic behavior in *Mtor*$^{flx/flx}$*:Vip-Cre* mice. The proportion of variance accounted for by the circadian component was lower in the *Mtor*$^{flx/flx}$*:Vip-Cre* mice than the *Mtor*$^{flx/flx}$ mice ($P = 0.055$; Fig. 2*D*), indicating more spread activities in LL in *Mtor*$^{flx/flx}$*:Vip-Cre* mice. Together, these results indicate more unstable and weakened rhythmicity of *Mtor*$^{flx/flx}$*:Vip-Cre* mice in LL.

Vip$^{-/-}$ and *VPAC2*$^{-/-}$ mice show dissociation of activities in a skeleton photoperiod (27, 28). To further assess the circadian clock function in *Mtor*$^{flx/flx}$*:Vip-Cre* mice and compare their phenotypes with those of *Vip*$^{-/-}$ and *VPAC2*$^{-/-}$ mice, the animals were exposed to a skeleton photoperiod, consisting of two 11-h dark periods separated by 1-h light periods (1-h/11-h/1-h/11-h LDLD). The amount of total activities during the skeleton photoperiod was not significantly different between the *Mtor*$^{flx/flx}$*:Vip-Cre* and *Mtor*$^{flx/flx}$ mice [*Mtor*$^{flx/flx}$*:Vip-Cre* vs. *Mtor*$^{flx/flx}$: 156 ± 13.2 revolutions (rev) per h, $n = 7$ vs. 133.8 ± 11.4 rev per h, $n = 5$, $t = 1.227$, $P = 0.248$]. Whereas *Mtor*$^{flx/flx}$ mice demonstrated an average of 77.9% of their total activity at the time corresponding to night in the 12-h/12-h LD cycle, *Mtor*$^{flx/flx}$*:Vip-Cre* mice restricted only 40.6% of their total activity to this period (Fig. 2 *E* and *F*). These results suggest that multiple oscillatory components exist in the clock of *Mtor*$^{flx/flx}$*:Vip-Cre* mice, one of which cannot be entrained by the 1-h/11-h/1-h/11-h LDLD cycle.

Circadian Synchrony Is Disrupted in the SCN of *Mtor*$^{flx/flx}$*:Vip-Cre* Mice. VIP mediates circadian synchrony among SCN neurons (21). To investigate the cellular basis underlying the abnormal circadian behavior in the *Mtor*$^{flx/flx}$*:Vip-Cre* mice, we crossed these mice to *PER2::LUCIFERASE* (PER2::LUC) mice (29). In PER2::LUC mice, the luciferase gene is fused to the endogenous clock gene Per2 to create a real-time reporter of dynamic circadian PER2 expression. As previously described (26), we performed microscopic bioluminescence imaging using SCN slices from the *PER2::LUC:Mtor*$^{flx/flx}$*:Vip-Cre* and *PER2::LUC:Mtor*$^{flx/flx}$ mice. The *Mtor*$^{flx/flx}$ SCN exhibited pronounced circadian cycles of PER2-driven bioluminescence from abundant bioluminescent regions of interest (ROIs; indicating rhythmic cells) (159 ± 70 ROIs per SCN from four slices). The cellular bioluminescence rhythms were highly synchronized from different ROIs, evident from raster plots (Fig. 3*A*, *Left*). In contrast, *Mtor*$^{flx/flx}$*:Vip-Cre* slices exhibited lower-intensity and fewer rhythmic ROIs across the SCN (106 ± 24 ROIs per SCN from six slices), which is consistent with decreased PER1 and PER2 levels in the SCN as determined by immunostaining (Fig. S2). In contrast to the highly synchronized bioluminescence rhythms of ROIs in the *Mtor*$^{flx/flx}$ slices, ROIs from the *Mtor*$^{flx/flx}$*:Vip-Cre* SCN were less well synchronized, especially during later cycles (Fig. 3*A*, *Right*). Next, we calculated the synchronization (sync) index for each slice, which quantifies the degree of phase clustering among cells, ranging from 0 (uniformly distributed phases across the day) to 1.0 (all cells peak at the same time of day) (30). We found that the sync index was significantly decreased in the SCN of *Mtor*$^{flx/flx}$*:Vip-Cre* mice (Fig. 3*C*).

To complement the genetic approach to knocking down *mTOR*, we examined the effects of an mTOR inhibitor, PP242, on SCN cell synchrony. PP242 is a potent, selective, and ATP-competitive mTOR inhibitor; 1 μM PP242 has been shown to significantly inhibit mTOR activities and perturb the translatome in cells (24). In contrast to cellular bioluminescence from slices treated with DMSO (CTR), rhythmic ROIs in PP242-treated SCN were less synchronized, with phases drifting apart over time (Fig. 3*B*). The sync index was significantly lower in PP242-treated SCN compared with controls (Fig. 3*D*). Moreover, the proportion of rhythmic ROIs (indicating rhythmic cells) was markedly lower in PP242-treated SCN explants (Fig. 3*E*), indicating that mTOR is also critical for cellular rhythmicity in the SCN. Together, these results demonstrate that mTOR controls synchrony of SCN cells at least partially through VIP neurons.

Odor Stimulates mTOR Activation in the Olfactory System. The olfactory bulb (OB) is another representative brain region where VIP neurons are enriched (23, 31, 32). Interestingly, VIP has been shown to mediate circadian rhythms in the OB (33). This prompted us to investigate the potential role for mTOR in olfaction using the *Mtor*$^{flx/flx}$*:Vip-Cre* mice.

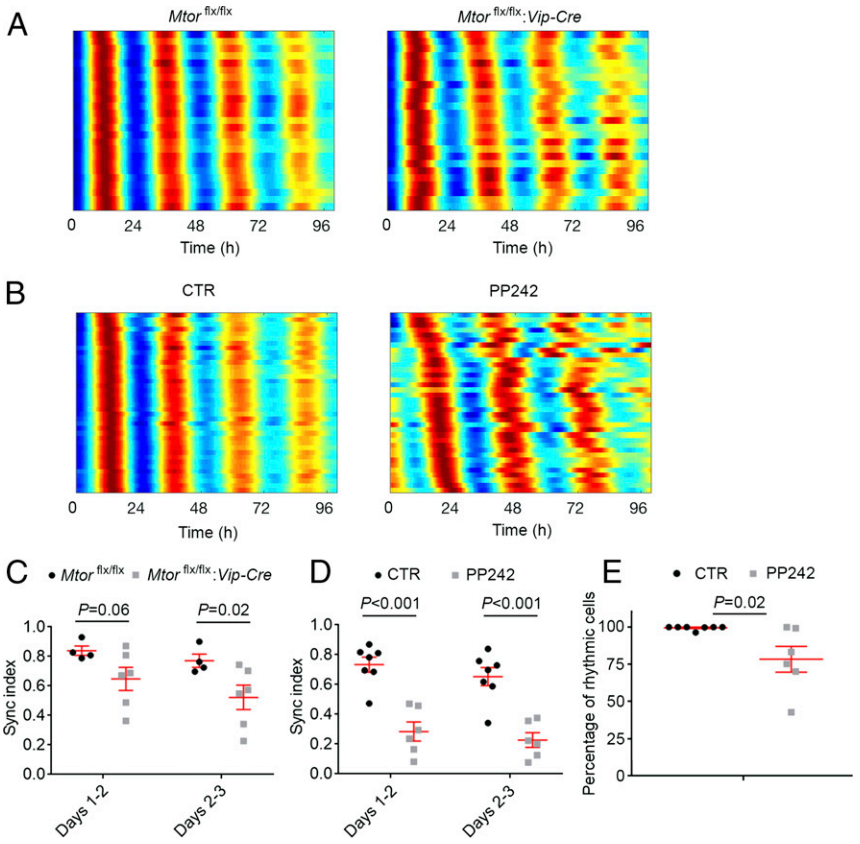

Fig. 3. mTOR inhibition desynchronizes SCN neurons. (*A*) Representative raster plots show the daily expression pattern of PER2::LUCIFERASE from 25 representative ROIs (indicators of rhythmic cells) in an SCN slice from an *Mtor*$^{flx/flx}$ (*Left*) or *Mtor*$^{flx/flx}$*:Vip-Cre* (*Right*) mouse. Note that the cellular rhythms of *Mtor*$^{flx/flx}$*:Vip-Cre* mice were more loosely synchronized compared with the *Mtor*$^{flx/flx}$ mice. (*B*) Representative raster plots show the daily expression pattern of PER2::LUCIFERASE from 25 representative ROIs in an SCN slice treated with DMSO (CTR) or the mTOR inhibitor PP242 (1 μM). Note that PP242 significantly disrupted synchronization of SCN cells. (*C* and *D*) Quantification of cellular synchronization within each slice using the synchronization index. (*E*) Percentages of rhythmic ROIs in DMSO (CTR) or PP242-treated SCN slices. Data in *C*–*E* are presented as individual values as well as mean ± SEM. For *C* and *D*, four *Mtor*$^{flx/flx}$ SCN slices and six *Mtor*$^{flx/flx}$*:Vip-Cre* slices were used in the experiment. For *E*, seven SCN slices were used for control and six slices were used for PP242 treatment.

Various odorants reach respective olfactory receptors on the olfactory receptor neurons, which project axons to separate glomeruli in the OB and synapse on mitral cells, the principal output neurons of the OB. Olfactory information from the OB is relayed to pyramidal cells in the piriform cortex (PIR). The anterior olfactory nucleus (AON) is also an olfactory relay station which has reciprocal connections with both the OB and PIR. We first examined the expression pattern of p-S6 and its regulation in these regions of *Mtor*$^{flx/flx}$ mice. p-S6 was expressed throughout all layers in the OB, including the periglomerular layer (PGL), external plexiform layer (EPL), mitral cell layer (MCL), and granule cell layer (GCL), as well as in the AON and PIR (Fig. S3). In the OB, p-S6 was enriched in the PGL, MCL, and GCL (Fig. S3*A*). To investigate potential regulation of mTOR activity by neuronal activities, mice were exposed to an odorant (eucalyptus essential oil) for 15 min at circadian time (CT)15 and killed 45 min after odor exposure. Immunostaining for p-S6 demonstrates that odor evoked significant up-regulation of S6 phosphorylation in the OB, AON, as well as PIR (Fig. S3 *A*, *B*, and *D*). Western blotting confirmed the immunostaining results that odor evoked p-S6 up-regulation in the OB (Fig. S3*C*).

As reported previously, VIP is extensively expressed in the PGL and EPL and sparsely in the GCL of the OB (31–33). Colocalization of VIP and p-S6 expression was seen in cells in the PGL and EPL (Fig. 4*A*). In *Mtor*$^{flx/flx}$*:Vip-Cre* mice, p-S6 expression was significantly reduced in the VIP-expressing EPL but not in the non–VIP-expressing MCL (Fig. 4*B*), indicating specific knockdown of *mTOR* in VIP neurons. Consistent with this, odor-evoked p-S6 up-regulation was abolished in the EPL of *Mtor*$^{flx/flx}$*:Vip-Cre* mice (Fig. 4*C*).

Olfaction Is Impaired in *Mtor*$^{flx/flx}$*:Vip-Cre* Mice. c-Fos is a marker of neuronal activation and has been shown to be induced by odor in the rodent olfactory system (34–37). To evaluate whether mTOR in VIP neurons mediates olfactory responses, we examined odor-induced c-Fos expression in *Mtor*$^{flx/flx}$ and *Mtor*$^{flx/flx}$*:Vip-Cre* mice. As previously reported (37), odor induced c-Fos expression in the OB, AON, and PIR (Fig. 5 *A*–*C*). Strikingly, c-Fos induction by odor was abolished in these regions in the *Mtor*$^{flx/flx}$*:Vip-Cre* mice (Fig. 5 *C* and *E*), indicating an essential role for mTOR signaling in mediating odor-stimulated neuronal responses in the olfactory system. To access the olfactory function of these mice, olfactory sensitivity to a neutral odor (cinnamon) was tested using a behavioral approach as previously described (38). Interestingly, *Mtor*$^{flx/flx}$*:Vip-Cre* mice exhibited decreased exploration time toward the odor compared with *Mtor*$^{flx/flx}$ littermates, which indicates decreased sensitivity to the odor. The minimum odor concentration to cause lengthened exploration was increased from 1:1,000 for *Mtor*$^{flx/flx}$ mice to 1:10 for *Mtor*$^{flx/flx}$*:Vip-Cre* mice (Fig. 5*F*).

Discussion

To study the physiological function of mTOR in the adult brain, we established a mouse model in which *mTOR* is specifically knocked down in VIP neurons. Using this model, we found that mTOR signaling in VIP neurons is critical for SCN cell synchronization and olfaction. Mice with decreased mTOR activities in VIP neurons show impaired circadian behavior, which can be mechanistically explained by weakened synchronization among SCN cells. These results are consistent with a role for mTOR in promoting *Vip* mRNA translation and decreased VIP levels in *mTOR* knockdown animals. Moreover, we found a key role for mTOR in mediating olfactory perception. mTOR activities in the olfactory system are stimulated by odor. *mTOR* knockdown in VIP neurons abolishes odor-evoked c-Fos expression in olfactory regions including the OB, AON, and PIR, which is consistent with reduced olfactory sensitivity in these animals. Together, these results highlight diverse physiological functions of mTOR in the adult brain.

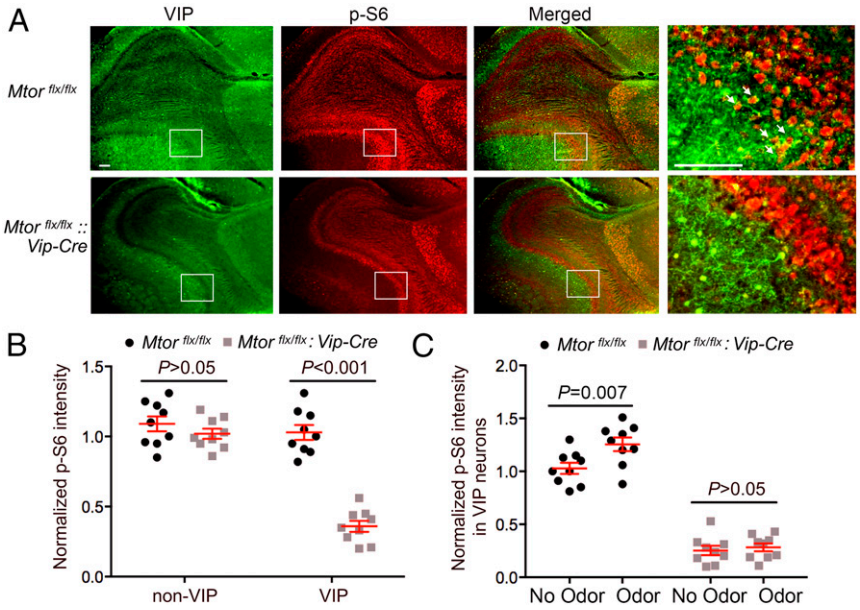

Fig. 4. mTOR signaling in the olfactory bulb. (*A*) Representative fluorescent microscopic images showing immunolabeling for VIP (green) and p-S6 (red) in the mouse OB. Framed regions are magnified and shown (*Right*) as a merged image. White arrows indicate cells expressing both p-S6 and VIP in the external plexiform layer. (Scale bars, 100 μm.) (*B*) Quantitation of p-S6 labeling intensity in the OB. Note that p-S6 level was markedly decreased in the VIP-expressing layer (EPL) but not in a non-VIP layer (mitral cell layer) in *Mtor*$^{flx/flx}$*:Vip-Cre* mice. (*C*) Quantitation of p-S6 labeling intensity in the OB. For this experiment, mice were exposed to an odorant (essence oil) for 15 min at CT15 and killed 45 min after the end of odor exposure. See *Materials and Methods* for detailed methods of quantitation. Note that odor evoked significant p-S6 up-regulation in the OB of *Mtor*$^{flx/flx}$ mice but not in *Mtor*$^{flx/flx}$*:Vip-Cre* mice. For *B* and *C*, data are presented as individual values as well as mean ± SEM. Three mice were included in each group and three brain sections were used from each animal.

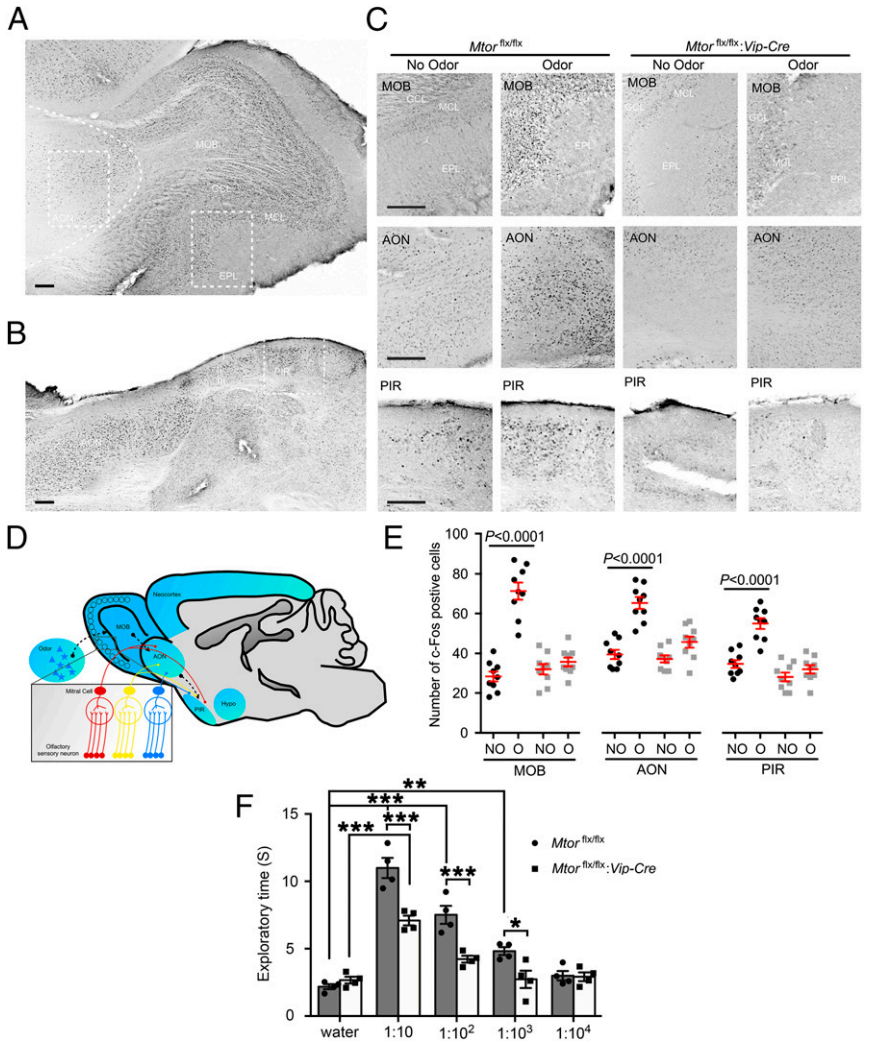

Fig. 5. Olfactory responses are blunted in *Mtor*$^{flx/flx}$*:Vip-Cre* mice. (*A* and *B*) Representative bright-field microscopic images of immunolabeling for c-Fos. Low-magnification images of the main olfactory bulb (*A*) and piriform cortex (*B*) from an odor-stimulated *Mtor*$^{flx/flx}$ mouse are shown. (Scale bars, 100 μm.) Curved dashed line indicates the border of the anterior olfactory nucleus. (*C*) High-magnification images of the MOB, anterior olfactory nucleus, and PIR from the framed regions in *A* and *B*. For this experiment, mice were exposed to an odorant for 15 min starting at CT15 and killed 45 min after the end of odor exposure. Note that odor evoked significant c-Fos expression in the MOB, AON, and PIR in *Mtor*$^{flx/flx}$ mice. c-Fos induction by odor in these regions was abolished in the *Mtor*$^{flx/flx}$*:Vip-Cre* mice. (Scale bars, 100 μm.) (*D*) A schematic diagram of the olfactory pathway. Briefly, various odorants reach different olfactory receptors on the olfactory receptor neurons, which project axons to separate glomeruli in the OB and synapse on mitral and tufted (M/T) cells. Olfactory information from the OB is relayed via M/T cell axons directly to pyramidal cells in the PIR. The AON has reciprocal connections with both the OB and PIR. (*E*) Numbers of c-Fos–positive cells per mm^2. See *Materials and Methods* for detailed methods of quantitation. Data are presented as individual values as well as mean ± SEM for each group. Three mice were included in each group and three brain sections were used from each animal. NO, no odor; O, odor. (*F*) Mouse exploratory time in the olfactory sensitivity test. Mice were exposed to one of four different dilutions of cinnamon extract on filter paper for a 3-min session. Total time spent exploring the filter paper was assessed. Note that the *Mtor*$^{flx/flx}$*:Vip-Cre* mice exhibited decreased olfactory sensitivity compared with the *Mtor*$^{flx/flx}$ mice. **P* < 0.05, ***P* < 0.01, ****P* < 0.001.

mTOR is ubiquitously expressed in the brain. mTOR signaling is increasingly found to be involved in unique neuronal activities. As constitutive *mTOR* knockout is embryonically lethal, studies of mTOR functions in the brain rely on conditional *mTOR* knockout models. The Cre-LoxP system is commonly used to circumvent embryonic lethality caused by systemic inactivation of a specific gene, since deletion of the gene occurs only in cells where Cre recombinase is expressed. It provides the best experimental control linking genotypes to phenotypes. In our study, *Mtor*$^{flx/flx}$*:Vip-Cre* mice were compared with *Mtor*$^{flx/flx}$ littermates. Of note, *Vip-Cre* is only expressed at the late embryonic to neonatal period, and thus it can be used to manipulate VIP neurons without disruption of their neural development (23). Indeed, the *Mtor*$^{flx/flx}$*:Vip-Cre* mice survived without visible deficits, and their brain histology is largely normal.

VIP is a peptide of 28 amino acid residues that belongs to a glucagon/secretin superfamily, the ligand of G protein-coupled receptors. *Vip* is expressed in a subset of GABAergic neurons in the neocortex, SCN, OB, and other midbrain and brainstem regions as well as the gut and pancreas (39–41). The direct protein product of the *Vip* gene is prepro-VIP, a 170-amino acid peptide. Our previous work discovered that mRNA translation of *Vip* is dependent on eIF4E and inhibited by 4E-BPs (20). Binding of 4E-BPs to eIF4E causes inhibition of cap-dependent translation initiation and is relieved when 4E-BPs are phosphorylated by mTOR. Thus, mTOR signaling promotes *Vip* mRNA translation (20). Knockdown of *mTOR* in VIP cells markedly decreased the level of prepro-VIP and VIP. Consistently, the mice exhibited significant circadian phenotypes, which largely resemble those seen in *Vip* or *VPAC2* null mice (27,

Table 1. Antibodies used for immunostaining and Western blotting

Antibody	Supplier	Catalog no.	Dilution in immunostaining	Dilution in Western blotting
VIP	Santa Cruz	sc-21041	1:200	
mTOR	Cell Signaling	2983		1:1,000
p-S6	Cell Signaling	2215	1:300	1:1,000
S6	Santa Cruz	74459		1:2,000
PER1	MilliporeSigma	AB2201	1:3,000	
PER2	Santa Cruz	SC-7728	1:300	
Prepro-VIP	Sigma-Aldrich	V0390		1:500
VPAC2	Abcam	ab28624		1:1,000
β-Actin	Sigma-Aldrich	A5441		1:5,000
c-Fos	Calbiochem	PC38	1:3,000	

28, 42, 43) as well as in rats treated with VIP antagonists (44). These phenotypes are (*i*) weakened circadian rhythmicity under constant conditions; (*ii*) disrupted circadian behavior under the skeleton photoperiod; and (*iii*) decreased synchrony among SCN cells. However, as a residual amount of VIP is still expressed in *Mtor*$^{flx/flx}$*:Vip-Cre* mice (possibly due to other translational control mechanisms and/or the mosaic pattern of *Vip-Cre* expression), the VIP-related circadian phenotypes are not as strong as those in *Vip* and *VPAC2* null mice.

Interestingly, the mTOR inhibitor PP242 has a similar, if not stronger, effect on SCN cell synchrony as VIP neuron-specific knockdown of mTOR. As mTOR inhibition by PP242 leads to decreased VIP expression (20), the effect of PP242 may be due to a decreased VIP level in the SCN. However, other mechanisms whereby mTOR regulates SCN cell synchrony cannot be excluded. For example, mTOR inhibition by rapamycin increases GABAergic synaptic transmission (45). As endogenous GABA has been shown to desynchronize circadian cells in the SCN (46), mTOR may also regulate synchrony through modifying GABAergic neurotransmission in the SCN.

mTOR regulates the circadian clock through complex mechanisms. In the current study, genetic and pharmacological inhibition of mTOR activity significantly reduced cellular synchronization as well as the number of rhythmic cells in the SCN. We previously demonstrated that rapamycin inhibits light-induced clock protein PER1 and PER2 expression in the SCN (19). A recent study pointed to the role for mTOR in regulating proteostasis of the clock protein BMAL1 (47). On the other hand, mTOR activity is rhythmically controlled by the circadian clock in the SCN. mTOR activity is high during the day and low at night, which is consistent with close cellular colocalized expression of p-S6 and *Per1* in the SCN (18). Light at night rapidly activates mTOR signaling in the SCN (17). Thus, the circadian clock controls the rhythmicity and activity of mTOR. In turn, mTOR signaling feeds back to the circadian clock to regulate its entrainment and synchronization. As mTOR forms a complex signaling network, further in vitro and in vivo studies using specific mutants of mTOR targets will be required to delineate the complex mechanisms whereby mTOR signaling interacts with the circadian clock.

In the current study, the function of mTOR was studied in the olfactory system. We found strong mTOR activities in all layers of the OB as well as in the AON and PIR. Moreover, mTOR activities are stimulated by odorants, and *mTOR* knockdown in VIP cells diminishes odor-evoked c-Fos responses in the olfactory system. The mechanisms whereby mTOR regulates olfactory c-Fos expression are not clear. A prominent feature of VIP interneurons is their preferential innervation of other interneurons (48, 49). VIP-containing cells in the EPL form an interneuronal network that modulates the function of other inhibitory interneurons (33, 50). VIP neurons may be involved in regulating network excitability and disinhibition of principal cells in the OB, which is similar to a role for VIP neurons in the cortex (51, 52). Thus, the EPL might serve as the "amplifier" of the incoming olfactory signal. mTOR signaling regulates neuronal excitability in cultured neurons (53, 54) as well as in epilepsy animal models (55). mTOR may regulate the excitability of VIP interneurons and therefore control olfactory input through the VIP interneuron network in the EPL. Further electrophysiological studies are required to test these hypotheses.

The regulation and functions of mTOR activity exhibit great similarities between the SCN and OB. First, the base level of mTOR activities is high in both regions. In the SCN, p-S6 expression shows circadian rhythmicity, with the peak level at CT12. Also, the SCN is the only brain region that exhibits a high level of phospho-4E-BPs, other downstream effectors of mTORC1. Second, mTOR activities are induced by neuronal activities in both regions. In the SCN, VIP cells are among the photic recipient neurons that receive direct synaptic input from the intrinsically photosensitive retinal ganglion cells. mTOR signaling is rapidly activated in these neurons by light stimulation at night. Similarly, odor stimulation activates mTOR in neurons in the OB. Third, mTOR exhibits similar functions in the SCN and OB in its regulation of neuronal network properties. In the SCN, VIP neurons are in the ventral region, but they form a neuronal network that couples and synchronizes the ventral and dorsal regions of the SCN. In the OB, VIP-expressing interneurons form a network in the EPL that is critical for controlling olfactory input. Thus, mTOR signaling regulates properties of structured VIP neuronal networks in the SCN and OB.

Materials and Methods

Animals. *Mtor*$^{flx/flx}$ mice on a C57BL/6 background kindly provided by Sara C. Kozma, University of Cincinnati, Cincinnati, OH, were crossed to a *Vip* promoter-driven Cre-recombinase mouse line (*Vip-Cre*; Jackson Laboratory) to generate *Mtor*$^{flx/flx}$*:Vip-Cre* mice. Mice were then crossed with *mPER2::LUC* transgenic reporter mice (29) to obtain *Mtor*$^{flx/flx}$*:Vip-Cre:mPER2::LUC* mice. Mice were maintained in the animal facilities at the University of Minnesota, Duluth Campus, McGill University, or Concordia University in accordance with institutional guidelines. All procedures were approved by the Institutional Animal Care and Use Committees at University of Minnesota, McGill University, and Concordia University.

Brain Tissue Processing, Immunostaining, and Microscopic Imaging Analysis. Under the indicated conditions, the mice were killed and brain tissue was harvested. Brain sections were processed and immunostained for p-S6, VIP, and c-Fos as previously reported (45). Bright-field and fluorescent microscopic images were captured using a digital camera mounted on an inverted DMi8 Leica microscope. Confocal microscopy images were captured using a Zeiss 710 Meta confocal microscope. See Table 1 for antibody information.

All photomicrographic datasets were statistically analyzed using Adobe Photoshop software (Adobe Systems). For the p-S6 and VIP colocalization assay, confocal SCN images (40× magnification) of double labeling for p-S6 and VIP were collected. Individual SCN cells were outlined based on DRAQ5 (a cell nuclear dye) staining, and the expression of p-S6 (red), VIP (green), or both (yellow) was determined based on densitometry values for red (p-S6)

and green (VIP) channels. The percentages of red, green, or yellow cells were calculated and compared between the *Mtor*$^{flx/flx}$ and *Mtor*$^{flx/flx}$*:Vip-Cre* mice.

For p-S6 intensity analysis, 20× fluorescent microscopic images of the main olfactory bulb (MOB) were acquired using a Leica DFC3000 G camera. All imaging parameters (exposure time, light intensity, etc.) were held constant for all datasets from the same experiment. Three digital squares (size 50 × 50 pixels) were randomly placed in VIP-positive or -negative regions and the mean labeling intensity of the three squares was determined. A digital square (size 50 × 50 pixels) was then placed in the outer layer of the cortex, where no p-S6 was expressed, to determine the intensity of nonspecific background staining. The background value was subtracted from the p-S6 labeling value to obtain the normalized p-S6 intensity. Three brain sections were used from each animal and three mice were used in each group.

For c-Fos–positive cell counting, 20× bright-field microscopic images were acquired from the MOB, AON, and PIR regions. Three digital squares (size 50 × 50 pixels) were randomly placed in one of these regions and an intensity threshold filter was applied to eliminate nonspecific background labeling. The total number of detectable signals within the square (indicating the number of positive cells) was determined by ImageJ (NIH), and the mean number from the three squares was used for each brain section. Three brain sections were used from each animal and three mice were used in each group.

Protein Extraction and Western Blotting Analysis. Total forebrain tissue was homogenized with a pestle grinder (Fisher Scientific) and lysed using a lysis buffer as previously reported (20). Western blotting analysis was performed and the intensity of the blots was analyzed as described (56). See Table 1 for antibody information.

Circadian Behavioral Assay. Eight- to 10-wk-old male mice were individually housed in cages equipped with running wheels. Wheel rotation was recorded using the VitalView program (Mini Mitter) or ClockLab software (Actimetrics) (45). The animals were entrained to a 12-h/12-h light/dark cycle for 9 d, released into constant dark for 7 d, and transferred back to 12-h/12-h LD for 10 d. On the 11th day the LD cycle was advanced 8 h, and animal behavior was recorded for 21 d following the LD cycle shift before the LD cycle was delayed for 8 h. Ten days later, animals were transferred to constant light and kept in LL (200 lx) for 35 d. In another experiment, the animals were entrained in a 12-h/12-h LD cycle for 10 d and transferred to a skeleton photoperiod consisting of two 11-h dark periods per d separated by 1-h light pulses. After 28 d in the skeleton photoperiod, mice were put into DD for 21 d. The actograms of wheel-running activities were analyzed using ActiView software (Mini Mitter) or ClockLab software.

To analyze activities in LL, a discrete wavelet transform (DWT) was applied to decompose time series into circadian and ultradian components, as described (57), using the WMTSA package (Charles R. Cornish; https://atmos.washington.edu/wmtsa/). The DWT partitions the variance into circadian (17 to 32 h) and ultradian (0 to 16 h) scales. The proportion of variance accounted for by the circadian scale indicates how well-consolidated activity is as a circadian rhythm. The time between peaks in the DWT circadian component can be used to estimate cycle length on each cycle; the SD of these cycle lengths indicates the variability in period over time. The DWT was applied to 21 d of activity under LL, starting 2 wk after mice were first transferred to LL.

Explant Culture, Kinetic Bioluminescence Imaging, and Data Analysis. Explants of SCN tissues from *Mtor*$^{flx/flx}$*:Vip-Cre:mPER2::LUC* and *Mtor*$^{flx/flx}$*:mPER2::LUC* mice were dissected and cultured as reported (26). For cellular-resolution real-time assays, coronal sections containing SCN were imaged as previously described (26). Briefly, sections containing SCN (150 μm) were collected, cultured on a membrane (Millicell CM; Millipore) in 1.2 mL of air-buffered media containing 0.1 mM beetle luciferin (Gold Biotechnology), and imaged for 5 d using a Stanford Photonics XR/MEGA-10Z cooled intensified charge-coupled device camera. For pharmacological experiments, the mTOR inhibitor PP242 or DMSO was added to respective culture media and dishes were imaged simultaneously.

Rhythmic parameters of PER2::LUC expression were calculated for each slice and for cell-like regions of interest (ROIs) within each slice using MATLAB (MathWorks)-based computational analyses as described previously (46). Briefly, phase maps of slices were constructed by generating a 4-d time series for each 12-pixel-diameter region of the image that met the criteria for circadian rhythmicity, namely a peak autocorrelation coefficient significant at alpha = 0.05 and associated with lag between 18 and 34 h. To locate and extract data from cell-like ROIs, an iterative process was employed after background and local noise subtraction of a slice image summed across 24 h of bioluminescence (26). The synchronization index R is computed as in equation 6 of ref. 30, using 2-d segments. To assess overall rhythmicity in each slice, 4-d time series were extracted for each of the 20% brightest pixels in each processed image (with bioluminescence summed across 24 h; a total of 5,369 pixels used for each slice) and evaluated for rhythmicity using the same criteria as above. The percentage of these pixels associated with a significantly rhythmic time series is used as a general estimate of what proportion of the slice is rhythmic. Because of small sample sizes and nonnormal distributions, permutation tests were used to test for significant difference in mean between groups. Raster plots show 36 cell-like ROIs chosen by sorting the first peak times and selecting 36 evenly spaced ROIs from the sorted list to obtain a more representative sample.

Odor Stimulation. Six- to 8-wk-old mice were entrained to a 12-h/12-h LD cycle for 14 d and transferred to constant darkness for 48 h. At CT15 the following day, mice were given olfactory stimulation consisting of a 15-min exposure to the odor of eucalyptus essential oil. Mice were killed 45 min after odor stimulation and brains were harvested and processed for immunostaining.

Olfactory Behavioral Test. Olfactory sensitivity was tested as described previously (38). Briefly, at zeitgeber time (ZT)15, 6- to 8-wk-old mice were exposed to one of four different dilutions of cinnamon extract (Watkins) or water on filter paper for a 3-min session. Total time spent exploring the filter paper was assessed.

Statistical Analysis. Values are presented as the mean ± SEM or percentage. Statistical analysis was performed using SPSS software (SPSS). Mean values from multiple groups were compared via one-way ANOVA, followed by Bonferroni's multiple comparisons. Mean values from two groups were compared via Student's t test. $P < 0.05$ was considered statistically significant.

ACKNOWLEDGMENTS. We thank Isaac Edery for critical reading of the manuscript, and Karthikeyan Ramanujam, Makenzie Morgen, and Mengmeng Tian for technical assistance. This study was supported by a Faculty Start-Up Grant from the University of Minnesota Medical School (to R.C.), Canadian Institutes of Health Research Grants MOP7214 (to N.S.) and MOP142458 (to S.A.), and NIH Grant SC1 GM112567 (to A.J.D.).

1. Wullschleger S, Loewith R, Hall MN (2006) TOR signaling in growth and metabolism. *Cell* 124:471–484.
2. Saxton RA, Sabatini DM (2017) mTOR signaling in growth, metabolism, and disease. *Cell* 168:960–976.
3. Ferrari S, Bandi HR, Hofsteenge J, Bussian BM, Thomas G (1991) Mitogen-activated 70K S6 kinase. Identification of in vitro 40 S ribosomal S6 phosphorylation sites. *J Biol Chem* 266:22770–22775.
4. Pende M, et al. (2004) S6K1(–/–)/S6K2(–/–) mice exhibit perinatal lethality and rapamycin-sensitive 5′-terminal oligopyrimidine mRNA translation and reveal a mitogen-activated protein kinase-dependent S6 kinase pathway. *Mol Cell Biol* 24:3112–3124.
5. Weng QP, et al. (1998) Regulation of the p70 S6 kinase by phosphorylation in vivo. Analysis using site-specific anti-phosphopeptide antibodies. *J Biol Chem* 273: 16621–16629.
6. Lipton JO, Sahin M (2014) The neurology of mTOR. *Neuron* 84:275–291.
7. Murakami M, et al. (2004) mTOR is essential for growth and proliferation in early mouse embryos and embryonic stem cells. *Mol Cell Biol* 24:6710–6718.
8. Gangloff YG, et al. (2004) Disruption of the mouse mTOR gene leads to early post-implantation lethality and prohibits embryonic stem cell development. *Mol Cell Biol* 24:9508–9516.
9. Banko JL, Hou L, Poulin F, Sonenberg N, Klann E (2006) Regulation of eukaryotic initiation factor 4E by converging signaling pathways during metabotropic glutamate receptor-dependent long-term depression. *J Neurosci* 26:2167–2173.
10. Hoeffer CA, et al. (2008) Removal of FKBP12 enhances mTOR-Raptor interactions, LTP, memory, and perseverative/repetitive behavior. *Neuron* 60:832–845.
11. Antion MD, Hou L, Wong H, Hoeffer CA, Klann E (2008) mGluR-dependent long-term depression is associated with increased phosphorylation of S6 and synthesis of elongation factor 1A but remains expressed in S6K-deficient mice. *Mol Cell Biol* 28: 2996–3007.
12. Huang W, et al. (2013) mTORC2 controls actin polymerization required for consolidation of long-term memory. *Nat Neurosci* 16:441–448.
13. Cota D, et al. (2006) Hypothalamic mTOR signaling regulates food intake. *Science* 312: 927–930.
14. Seibt J, et al. (2012) Protein synthesis during sleep consolidates cortical plasticity in vivo. *Curr Biol* 22:676–682.
15. Tudor JC, et al. (2016) Sleep deprivation impairs memory by attenuating mTORC1-dependent protein synthesis. *Sci Signal* 9:ra41.
16. Santini E, Klann E (2014) Reciprocal signaling between translational control pathways and synaptic proteins in autism spectrum disorders. *Sci Signal* 7:re10.

17. Cao R, Lee B, Cho HY, Saklayen S, Obrietan K (2008) Photic regulation of the mTOR signaling pathway in the suprachiasmatic circadian clock. *Mol Cell Neurosci* 38: 312–324.
18. Cao R, Anderson FE, Jung YJ, Dziema H, Obrietan K (2011) Circadian regulation of mammalian target of rapamycin signaling in the mouse suprachiasmatic nucleus. *Neuroscience* 181:79–88.
19. Cao R, Li A, Cho HY, Lee B, Obrietan K (2010) Mammalian target of rapamycin signaling modulates photic entrainment of the suprachiasmatic circadian clock. *J Neurosci* 30:6302–6314.
20. Cao R, et al. (2013) Translational control of entrainment and synchrony of the suprachiasmatic circadian clock by mTOR/4E-BP1 signaling. *Neuron* 79:712–724.
21. Aton SJ, Herzog ED (2005) Come together, right...now: Synchronization of rhythms in a mammalian circadian clock. *Neuron* 48:531–534.
22. Tsien JZ, et al. (1996) Subregion- and cell type-restricted gene knockout in mouse brain. *Cell* 87:1317–1326.
23. Taniguchi H, et al. (2011) A resource of Cre driver lines for genetic targeting of GABAergic neurons in cerebral cortex. *Neuron* 71:995–1013, and erratum (2011) 72:1091.
24. Larsson O, et al. (2012) Distinct perturbation of the translatome by the antidiabetic drug metformin. *Proc Natl Acad Sci USA* 109:8977–8982.
25. Daan S, Pittendrigh CS (1976) A functional analysis of circadian pacemakers in nocturnal rodents. *J Comp Physiol* 106:253–266.
26. Evans JA, Leise TL, Castanon-Cervantes O, Davidson AJ (2011) Intrinsic regulation of spatiotemporal organization within the suprachiasmatic nucleus. *PLoS One* 6:e15869.
27. Colwell CS, et al. (2003) Disrupted circadian rhythms in VIP- and PHI-deficient mice. *Am J Physiol Regul Integr Comp Physiol* 285:R939–R949.
28. Aton SJ, Colwell CS, Harmar AJ, Waschek J, Herzog ED (2005) Vasoactive intestinal polypeptide mediates circadian rhythmicity and synchrony in mammalian clock neurons. *Nat Neurosci* 8:476–483.
29. Yoo SH, et al. (2004) PERIOD2:LUCIFERASE real-time reporting of circadian dynamics reveals persistent circadian oscillations in mouse peripheral tissues. *Proc Natl Acad Sci USA* 101:5339–5346.
30. Gonze D, Bernard S, Waltermann C, Kramer A, Herzel H (2005) Spontaneous synchronization of coupled circadian oscillators. *Biophys J* 89:120–129.
31. Gall C, Seroogy KB, Brecha N (1986) Distribution of VIP- and NPY-like immunoreactivities in rat main olfactory bulb. *Brain Res* 374:389–394.
32. Gracia-Llanes FJ, Crespo C, Blasco-Ibáñez JM, Marqués-Marí AI, Martínez-Guijarro FJ (2003) VIP-containing deep short-axon cells of the olfactory bulb innervate interneurons different from granule cells. *Eur J Neurosci* 18:1751–1763.
33. Miller JE, et al. (2014) Vasoactive intestinal polypeptide mediates circadian rhythms in mammalian olfactory bulb and olfaction. *J Neurosci* 34:6040–6046.
34. Onoda N (1992) Odor-induced fos-like immunoreactivity in the rat olfactory bulb. *Neurosci Lett* 137:157–160.
35. Guthrie KM, Anderson AJ, Leon M, Gall C (1993) Odor-induced increases in c-fos mRNA expression reveal an anatomical "unit" for odor processing in olfactory bulb. *Proc Natl Acad Sci USA* 90:3329–3333.
36. Amir S, Cain S, Sullivan J, Robinson B, Stewart J (1999) In rats, odor-induced Fos in the olfactory pathways depends on the phase of the circadian clock. *Neurosci Lett* 272: 175–178.
37. Funk D, Amir S (2000) Circadian modulation of fos responses to odor of the red fox, a rodent predator, in the rat olfactory system. *Brain Res* 866:262–267.
38. Witt RM, Galligan MM, Despinoy JR, Segal R (2009) Olfactory behavioral testing in the adult mouse. *J Vis Exp* (23):949.
39. Gozes I (2008) VIP, from gene to behavior and back: Summarizing my 25 years of research. *J Mol Neurosci* 36:115–124.
40. Fahrenkrug J (2010) VIP and PACAP. *Results Probl Cell Differ* 50:221–234.
41. Waschek JA (2013) VIP and PACAP: Neuropeptide modulators of CNS inflammation, injury, and repair. *Br J Pharmacol* 169:512–523.
42. Harmar AJ, et al. (2002) The VPAC(2) receptor is essential for circadian function in the mouse suprachiasmatic nuclei. *Cell* 109:497–508.
43. Maywood ES, et al. (2006) Synchronization and maintenance of timekeeping in suprachiasmatic circadian clock cells by neuropeptidergic signaling. *Curr Biol* 16: 599–605.
44. Gozes I, et al. (1995) Superactive lipophilic peptides discriminate multiple vasoactive intestinal peptide receptors. *J Pharmacol Exp Ther* 273:161–167.
45. Weston MC, Chen H, Swann JW (2012) Multiple roles for mammalian target of rapamycin signaling in both glutamatergic and GABAergic synaptic transmission. *J Neurosci* 32:11441–11452.
46. Evans JA, Leise TL, Castanon-Cervantes O, Davidson AJ (2013) Dynamic interactions mediated by nonredundant signaling mechanisms couple circadian clock neurons. *Neuron* 80:973–983.
47. Lipton JO, et al. (2017) Aberrant proteostasis of BMAL1 underlies circadian abnormalities in a paradigmatic mTOR-opathy. *Cell Rep* 20:868–880.
48. Dávid C, Schleicher A, Zuschratter W, Staiger JF (2007) The innervation of parvalbumin-containing interneurons by VIP-immunopositive interneurons in the primary somatosensory cortex of the adult rat. *Eur J Neurosci* 25:2329–2340.
49. Somogyi P, et al. (2003) High level of mGluR7 in the presynaptic active zones of select populations of GABAergic terminals innervating interneurons in the rat hippocampus. *Eur J Neurosci* 17:2503–2520.
50. Schneider SP, Macrides F (1978) Laminar distributions of internuerons in the main olfactory bulb of the adult hamster. *Brain Res Bull* 3:73–82.
51. Lee S, Kruglikov I, Huang ZJ, Fishell G, Rudy B (2013) A disinhibitory circuit mediates motor integration in the somatosensory cortex. *Nat Neurosci* 16:1662–1670.
52. Jackson J, Ayzenshtat I, Karnani MM, Yuste R (2016) VIP+ interneurons control neocortical activity across brain states. *J Neurophysiol* 115:3008–3017.
53. Rüegg S, Baybis M, Juul H, Dichter M, Crino PB (2007) Effects of rapamycin on gene expression, morphology, and electrophysiological properties of rat hippocampal neurons. *Epilepsy Res* 77:85–92.
54. Niere F, Raab-Graham KF (2017) mTORC1 is a local, postsynaptic voltage sensor regulated by positive and negative feedback pathways. *Front Cell Neurosci* 11:152.
55. Cao R, Li A, Cho HY (2009) mTOR signaling in epileptogenesis: Too much of a good thing? *J Neurosci* 29:12372–12373.
56. Cao R, et al. (2015) Light-regulated translational control of circadian behavior by eIF4E phosphorylation. *Nat Neurosci* 18:855–862.
57. Leise TL, Harrington ME (2011) Wavelet-based time series analysis of circadian rhythms. *J Biol Rhythms* 26:454–463.